REVIEW ARTICLE

Investigation of Electron-Irradiation Damage in Silicon Carbide by Hall-Effect Measurements

Hideharu Matsuura

Affiliation:

Department of Electrical and Electronic Engineering, Osaka Electro-Communication University, Osaka 572-8530, Japan

Correspondence address: matsuura@osakac.ac.jp

Abstract

We review changes of the majority-carrier concentration and mobility in SiC by irradiation of high-energy electrons using Hall-effect measurements. The hole concentration (p) in Al-doped p-type SiC is decreased by irradiation of electrons with over 150 keV. This decrement of p is found to result from a decrement of Al acceptors with an acceptor level (E_A) of $E_V + 0.22$ eV. Because the irradiation of electrons with approximately 200 keV can displace only C atoms at lattice sites, neither Si nor Al atoms, one of four C atoms bonded with an Al atom at a Si-sublattice site is displaced by the irradiation, resulting that the Al atom at the Si-sublattice site cannot behave as a shallow acceptor, and is changed to a deep acceptor with E_A of $E_V + 0.38$ eV. In N-doped n-type SiC, the density of N donors at hexagonal C-sublattice sites with a donor level (E_D) of $E_C - 0.07$ eV is reduced much more than the density of N donors at cubic C-sublattice sites with E_D of $E_C - 0.12$ eV.

Keywords: Electron irradiation; Irradiation damage; Silicon Carbide; 4H-SiC; 6H-SiC; Majority-carrier concentration; Majority-carrier mobility

1. Introduction

Silicon carbide (SiC) is a wide bandgap semiconductor with significant potential for applications in high power and high frequency devices capable of operation at elevated temperatures. For electrons with energies greater than 500 keV, minority-carrier-lifetime degradation

Copyright 2017 KEI Journals. All Rights Reserved

by electron irradiation in SiC was reported to be lower than that in gallium arsenide (GaAs) by more than three orders of magnitude, and lower than that in silicon (Si) by at least one order of magnitude.[1] This indicates the greatly superior resistance of SiC to displacement damage in radiation environments.

Electron irradiation is an excellent tool for the controlled generation of intrinsic defects in Si for use in high power devices.[2] On the other hand, electron irradiation degrades the conversion efficiency of Si solar cells, for example such as those used in space applications.[3] Therefore, electron-radiation damage in Si has been intensively investigated in the past.[3-6] On the other hand, ion-implantation-induced defects in 4H-SiC epilayers have been reported.[7,8] However, the understanding of electron-irradiation damage in SiC is far from complete.

By comparing electron-irradiation damage in 4H-SiC with that in Si,[6,9,10] it was found that the reduction in the temperature dependence of the hole concentration $p(T)$ in aluminum (Al)-doped p-type 4H-SiC by electron irradiation was much larger than that in Al-doped p-type Si,[11] even though the electron energy (500 keV) and fluence ($0.5\times10^{15}\,\mathrm{cm}^{-2}$) used for the SiC were less than those (1MeV and $1\times10^{16}\,\mathrm{cm}^{-2}$) used for the Si.

The reduction in $p(T)$ in boron (B)-doped or gallium (Ga)-doped p-type Si was found to be similar to that in Al-doped Si.[6] Moreover, $p(T)$ in Al-doped 4H-SiC irradiated with a $1\times10^{16}\,\mathrm{cm}^{-2}$ fluence of 0.5 or 1 MeV electrons could not be measured because of the much higher resistivity of the irradiated samples.[10] Since the large reduction in $p(T)$ in Al-doped 4H-SiC by the electron irradiation was an unexpected result, the reduction in $p(T)$ by irradiation with different electron energies was investigated.[9-12]

The densities and energy levels of traps (or defects) have usually been evaluated using deep level transient spectroscopy (DLTS). However, a quantitative relationship between $p(T)$ and the trap densities cannot be obtained using DLTS. The reason for this is that in the DLTS analysis, the following approximation is assumed.[13-15]

$$C(t) = C(\infty)\sqrt{1-\frac{N_\mathrm{T}}{N_\mathrm{Dopant}+N_\mathrm{T}}\exp\left(-\frac{1}{\tau_\mathrm{T}}\right)} \cong C(\infty)\left[1-\frac{N_\mathrm{T}}{2\left(N_\mathrm{Dopant}+N_\mathrm{T}\right)}\exp\left(-\frac{1}{\tau_\mathrm{T}}\right)\right] \quad (1)$$

when

$$\frac{N_\mathrm{T}}{N_\mathrm{Dopant}+N_\mathrm{T}} << 1 \quad (2)$$

where $C(t)$ is the transient capacitance of a pn diode or a Schottky barrier diode after removal of the filling pulse and return to the steady-state reverse bias voltage in the DLTS measurement sequence, $C(\infty)$ is the steady-state capacitance, N_dopant is the dopant density

Copyright 2017 KEI Journals. All Rights Reserved

(i.e., donor or acceptor density), N_T is the trap density, and τ_T is the time constant corresponding to the trap. Based on Eq. (2), DLTS can determine the density and energy level of the trap only when N_T is much lower than N_{dopant}, indicating that the trap determined by DLTS barely affects $p(T)$. Moreover, transient capacitance methods (e.g., DLTS and isothermal capacitance transient spectroscopy) cannot be applied to high-resistivity semiconductors such as heavily-irradiated semiconductors because the measured capacitance of a diode is determined by the thickness of the diode, not by the depletion region of the junction due to its long dielectric relaxation time.[16-21]

The van der Pauw method can evaluate resistivity ($\rho(T)$) and the Hall-effect measurement can measure a Hall voltage ($V_H(T)$). From $V_H(T)$, the temperature dependence of the majority-carrier concentration (holes: $p(T)$ or electrons: $n(T)$) can be determined. Then, from $\rho(T)$ and $p(T)$ (or $n(T)$), the temperature dependence of the majority-carrier mobility (holes: $\mu_h(T)$ or electrons: $\mu_e(T)$) can be obtained.

If the densities and energy levels of dopants and traps can be determined using experimental $p(T)$ or $n(T)$, the relationship between $p(T)$ (or $n(T)$) and both the dopant density and the trap densities can directly be investigated. For the analysis of $p(T)$ or $n(T)$, a graphical peak analysis method (FCCS: free carrier concentration spectroscopy) has been proposed and tested,[15,22-28] which can determine the densities and energy levels of dopants and traps from experimental $p(T)$ or $n(T)$ without any assumptions regarding dopant species and traps.

The experimental $\mu_h(T)$ or $\mu_e(T)$ can be compared with five mobility components simulated from scattering mechanisms due to ionized impurities, neutral impurities, acoustic phonons, polar optical phonons, and nonpolar optical phonons,[29] and the origin of the degradation of the experimental mobility by electron irradiation can be investigated.

In this paper, we review electron-irradiation damage in SiC using the temperature dependencies of the majority-carrier concentration and majority-carrier mobility measured by the Hall-effect measurement.[9-12,30-34]

2. Experiments and Analyses

The temperature dependencies of $p(T)$ and $\mu_h(T)$ (or $n(T)$ and $\mu_e(T)$) were obtained by Hall-effect measurements in the van der Pauw configuration within the temperature range of 80 to 650 K in a magnetic field of 1.4 T using a modified MMR Technologies' Hall system. At room temperature, samples were irradiated by high-energy electrons.

The densities and energy levels of

Copyright 2017 KEI Journals. All Rights Reserved

dopants and traps can be determined by FCCS from the temperature dependent majority-carrier concentration. Using the experimental $p(T)$ or $n(T)$, the FCCS signal is defined as[15,22-28]

$$H(T,E_{\mathrm{ref}}) \equiv \frac{p(T)^2}{(k_{\mathrm{B}}T)^{5/2}} \exp\left(\frac{E_{\mathrm{ref}}}{k_{\mathrm{B}}T}\right) \quad (3a)$$

or

$$H(T,E_{\mathrm{ref}}) \equiv \frac{n(T)^2}{(k_{\mathrm{B}}T)^{5/2}} \exp\left(\frac{E_{\mathrm{ref}}}{k_{\mathrm{B}}T}\right), \quad (3b)$$

where k_{B} is the Boltzmann constant and E_{ref} is the parameter that can shift the peak temperature of the FCCS signal within the temperature range of the measurement. The FCCS signal has a peak at the temperature corresponding to each dopant level or trap level. From each peak, the density and energy level of the corresponding dopant or trap can be accurately determined. The application software for FCCS (for the Windows operating system) can be downloaded for free at our web-site (http://www.osakac.ac.jp/labs/matsuura/).

3. Results and Discussion

3.1. Al-doped 4H-SiC Epilayers

A 10-μm-thick Al-doped p-type 4H-SiC epilayer on n^+-type 4H-SiC (thickness: 376 μm, with a resistivity of 0.02 Ω·cm) was cut to a size of 1×1 cm^2. Four ohmic metal (Ti/Al) dots were deposited by a sputtering method on the four corners of the surface of the sample, and then the sample was annealed at 900 °C for 1 min in an Ar atmosphere. The $p(T)$ and $\mu_{\mathrm{h}}(T)$ were measured before irradiation, and then the sample was irradiated. After the Hall-effect measurement was carried out, the sample was again irradiated. The Hall-effect measurement and electron-irradiation were repeated. In this paper, a fluence of electrons (Φ) means the total fluence. Although the Hall-effect measurements were carried out twice for each Φ, the $p(T)$ remained unchanged, indicating that any defects affecting the $p(T)$ were not annealed at all for measurement temperature lower than 650 K.

Figure 1 shows the changes of $p(T)$ by electron irradiation with energies of 100, 150, 200, 500, and 4600 keV and several fluences. By 100 keV electron irradiation, the $p(T)$ was slightly increased, suggesting that the sample was considered to be annealed by heat due to the electron irradiation. By irradiation of 150 keV electrons with the fluence of 1×10^{16} cm^{-2}, the $p(T)$ was slightly increased, while the $p(T)$ was slightly

Copyright 2017 KEI Journals. All Rights Reserved

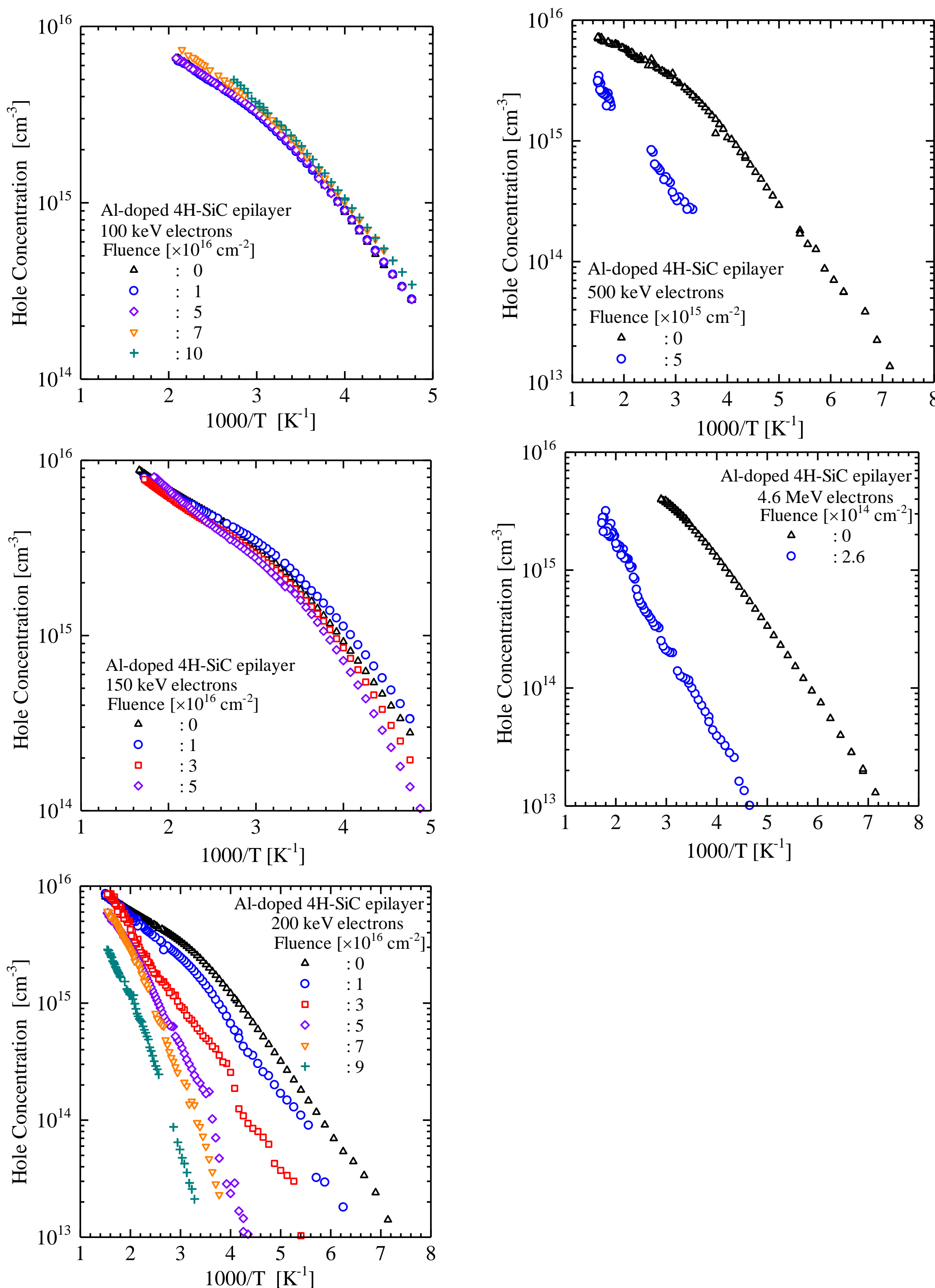

Figure 1. Changes of $p(T)$ by electron irradiation with several electron energies and several fluences.

Copyright 2017 KEI Journals. All Rights Reserved

decreased with the fluences of $\geq 2\times10^{16}$ cm^{-2}. Even with the 1×10^{16} cm^{-2} fluence of 200 keV electrons, the $p(T)$ was decreased. By irradiation of 500 keV electrons even with the fluence of 5×10^{15} cm^{-2} or by irradiation of 4600 keV electrons even with the fluence of 2.6×10^{14} cm^{-2}, the $p(T)$ was significantly decreased.

In the samples before and after irradiation, the values of the density (N_{Al}) and energy level (E_{Al}) of a shallow acceptor, the density (N_{DA}) and energy level (E_{DA}) of a deep acceptor, and a compensating density (E_{comp}) were determined by FCCS.

Figure 2 shows the relationship between N_{Al} and N_{DA} in unirradiated epilayers, and irradiated samples with several electron energies and several fluences.

The shallow acceptor level was approximately $E_{\mathrm{V}}+0.22$ eV, while the deep acceptor level was approximately $E_{\mathrm{V}}+0.38$ eV, where E_{V} is the top of the valence band. The former acceptor species is assigned to an Al acceptor (Al_{Si}) at a Si-sublattice site from photoluminescence[35] and Hall-effect[36] measurements, while the latter acceptor species is not assigned.

The origin of the deep acceptor is considered. Boron (B) in 4H–SiC was reported to form two electrical levels in the lower half of its bandgap.[37] One is located at approximately $E_{\mathrm{V}}+0.30$ eV as determined by Hall-effect

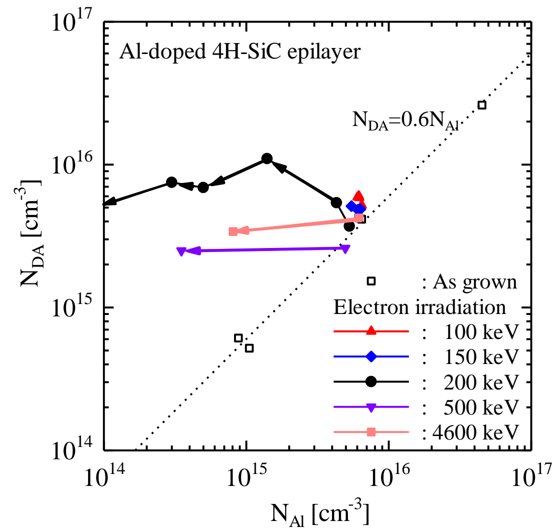

Figure 2. Relationship between N_{Al} and N_{DA} in unirradiated epilayers, and irradiated samples with several electron energies and several fluences.

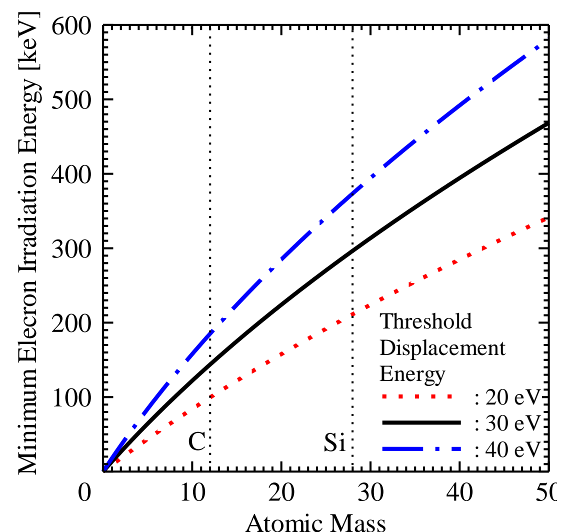

Figure 3. Dependencies of minimum electron irradiation energies on atomic mass at three threshold displacement energies.

Copyright 2017 KEI Journals. All Rights Reserved

measurements,[37] and the other is between $E_V + 0.55$ and $E_V + 0.60$ eV as determined by DLTS.[38] The shallow acceptor is assigned to a B atom (B_{Si}) at a Si-sublattice site. The probable identification of the deep acceptor is a complex (B_{Si}-V_C) of B_{Si} and its nearest neighbor C vacancy (V_C).[39,40]

In this study, although one of the possible origins of the unknown deep acceptor is B with which 4H–SiC is sometimes contaminated,[37-39] the concentration of B in the Al-doped 4H-SiC epilayers, which was measured by secondary ion mass spectroscopy (SIMS), was lower than 4×10^{14} cm^{-3}, indicating that B is not related to the deep acceptor.

In Fig. 2, the relationships between N_{Al} and N_{DA} in unirradiated epilayers with several doping densities are denoted by open squares, which were reported previously.[10,24] Because the empirical relationship in the unirradiated epilayers is obtained from Fig. 2 as

$$N_{DA} = 0.6 \times N_{Al}, \tag{4}$$

the deep acceptor should be related to Al.

By analogy with B in 4H–SiC, the deep acceptor in Al-doped 4H–SiC may be a complex (Al_{Si}-V_C) of an Al_{Si} and its nearest neighbor V_C, which was detected by electron paramagnetic resonance (EPR) spectroscopy.[40] It may be closely linked with the *D1* line observed by PL.[41]

The maximum energy (E_{max}) transferred from an irradiated electron with an energy (E_{ir}) to a nucleus is given by[42]

$$E_{max} = \frac{2E_{ir}\left(E_{ir} + 2m_e c^2\right)}{Mc^2}, \tag{4}$$

where M is the atomic mass, m_e is the electron rest mass, and c is the velocity of light. This indicates that an atom at a sublattice site is displaced by the irradiated electron when E_{max} is greater than the threshold displacement energy (E_d). Therefore, the minimum irradiation electron energy ($E_{ir\text{-}min}$) required to displace an atom at a sublattice site is the E_{ir} at $E_{max} = E_d$, and the relationship between $E_{ir\text{-}min}$ and M is given by

$$E_{ir\text{-}min} = \frac{2m_e c^2 + \sqrt{\left(2m_e c^2\right)^2 + 2Mc^2 E_d}}{2}. \tag{5}$$

Since the atomic mass of C is smaller than that of Si, the maximum energy transferred from an electron to one C atom at a sublattice site (C_s) in SiC by elastic collision is larger than the energy transferred to one Si atom at a sublattice site (Si_s).

In the sample irradiated by 100 keV electrons, the values of N_{Al} and N_{DA} were almost unchanged. By 150 keV electron irradiation, the change of N_{Al} was a little. On the other hand, N_{Al} was significantly decreased by ≥ 200 keV electron irradiation.

Equation (5) indicates that the minimum energy of irradiated electrons, which is necessary for displacing C_s,

Copyright 2017 KEI Journals. All Rights Reserved

should be much lower than those for displacing Si_s and Al_{Si}. According to experimental and theoretical considerations,[1,10,43-46] the value of E_d was approximately 40 eV in SiC. In this study, on the other hand, because N_{Al} was slightly decreased by 150 keV electron irradiation, E_d is considered to be between 30 eV and 40 eV. Alternatively, E_d for C_s bonded with one Al_{Si} and three Si_s is considered to be lower than 40 eV if it is correct that E_d for C_s bonded with four Si_s is 40 eV. This indicates that 200 keV electrons can only displace C_s in SiC, neither Si_s nor Al_{Si}. Therefore, we have mainly investigated the reduction in $p(T)$ in Al-doped p-type 4H-SiC by the irradiation of 200 keV electrons at several fluences.

3.1.1. 200 keV Electron Irradiation

3.1.1.1. Hole Concentration

Figure 4 shows the experimental $p(T)$ for Φ of 0, 1×10^{16}, 3×10^{16}, 5×10^{16}, 7×10^{16}, and 9×10^{16} cm^{-2}, denoted by triangles, circles, squares, diamonds, inverse triangles, and crosses, respectively. The $p(T)$ at low temperatures decreased significantly with increasing Φ, whereas the $p(T)$ at high temperatures was changed slightly by the irradiation.

The values of N_{Al}, E_{Al}, N_{DA}, E_{DA}, and E_{comp} were determined by FCCS using the experimental $p(T)$. The $p(T)$ was numerically simulated by using the following equations:

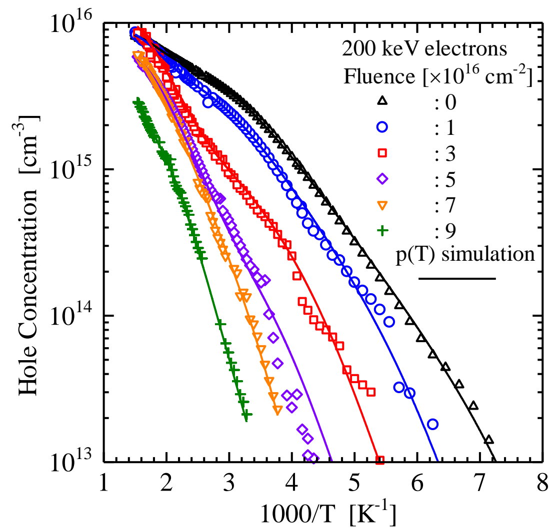

Figure 4. Temperature dependencies of hole concentrations for Al-doped 4H-SiC before and after irradiation with 200 keV electrons at five different fluences.

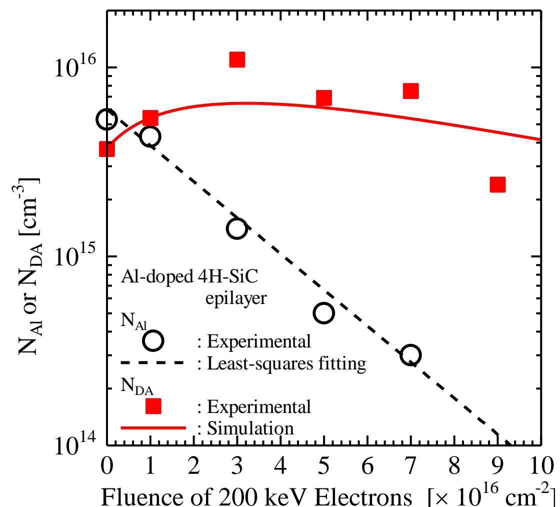

Figure 5. Fluence dependencies of shallow and deep acceptor densities.

Copyright 2017 KEI Journals. All Rights Reserved

$$p(T)+N_{\mathrm{comp}}=N_{\mathrm{Al}}f_{\mathrm{FD,A}}(E_{\mathrm{Al}},T)+N_{\mathrm{DA}}f_{\mathrm{FD,A}}(E_{\mathrm{DA}},T) \quad (6)$$

and

$$p(T)=N_{\mathrm{V}}(T)\exp\left[-\frac{E_{\mathrm{F}}(T)-E_{\mathrm{V}}}{k_{\mathrm{B}}T}\right], \quad (7)$$

where $f_{\mathrm{FD,A}}(E,T)$ is the Fermi-Dirac distribution function for acceptors, given by

$$f_{\mathrm{FD,A}}(E,T)=\frac{1}{1+g_{\mathrm{A}}\exp\left[\frac{E-E_{\mathrm{F}}(T)}{k_{\mathrm{B}}T}\right]}, \quad (8)$$

g_{A} is the degeneracy factor for acceptors, expressed as

$$g_{\mathrm{A}}=4, \quad (9)$$

and $N_{\mathrm{V}}(T)$ is the effective density of states in the valence band, which is given by

$$N_{\mathrm{V}}(T)=2\left(\frac{2\pi m_{\mathrm{h}}^{*}k_{\mathrm{B}}T}{h^{2}}\right)^{3/2} . \quad (10)$$

Here, $E_{\mathrm{F}}(T)$ is the Fermi level at T, m_{h}^{*} is the hole effective mass for the semiconductor, and h is Planck's constant. Each solid line in Fig. 4 is the result of a $p(T)$ simulation using the values of N_{Al}, E_{Al}, N_{DA}, E_{DA}, and N_{comp} for the corresponding Φ. The simulations are in good agreement with the corresponding experimental results.

At Φ of $\leq 7\times10^{16}$ cm^{-2}, two types of acceptor species were detected. At Φ of 9×10^{16} cm^{-2}, only the deep acceptor was detected because N_{Al} was much lower than N_{DA}. Figure 5 depicts the fluence dependencies of N_{Al} and N_{DA}. N_{Al} decreased with increasing Φ, and finally there are no more Al acceptors. On the other hand, N_{DA} initially increased with Φ, and then decreased.

In order to reduce N_{Al} by the 200 keV electron irradiation, the surroundings of the Al acceptor need to be changed by the displacement of one of four C_s bonded with Al_{Si}. This indicates that the rate of decrease of N_{Al} by the irradiation is proportional to N_{Al}. Consequently, the differential equation that leads to fluence dependence of the Al acceptor density, $N_{\mathrm{Al}}(\Phi)$, is given by

$$\frac{\mathrm{d}N_{\mathrm{Al}}(\Phi)}{\mathrm{d}\Phi}=-\kappa_{\mathrm{Al200}}N_{\mathrm{Al}}(\Phi), \quad (11)$$

where κ_{Al200} is the removal coefficient (or removal cross-section) of Al acceptors for 200 keV electron irradiation. Therefore,

$$N_{\mathrm{Al}}(\Phi)=N_{\mathrm{Al}}(0)\exp(-\kappa_{\mathrm{Al200}}\Phi). \quad (12)$$

In Fig. 5, a straight broken line is obtained by least-squares fitting. Since the straight line is in good agreement with the circles in the semi-logarithmic plots, Eq. (12) is applicable for the fluence dependence of N_{Al}. κ_{Al200} is then determined from the slope as 4.4×10^{-17} cm^{2}. Since by irradiation of 1 MeV electrons the removal coefficient of B acceptors in p-type Si with a B-doping concentration of 2×10^{16} cm^{-3} was reported to be approximately 8×10^{-18} cm^{2},[6] the electron-irradiation resistance of

Copyright 2017 KEI Journals. All Rights Reserved

p-type 4H-SiC is inferior to that of p-type Si.

In Fig. 5, at Φ of $\leq 3\times10^{16}$ cm^{-2}, N_{DA} increased with increasing Φ, while N_{Al} decreased. Furthermore, the increment of N_{DA} is close to the decrement of N_{Al}. This experimental result may indicate that the 200 keV electron irradiation transforms the Al acceptor (Al_{Si}) into the deep acceptor (Al_{Si}-V_C). On the other hand, N_{DA} is assumed to be decreased by the change of the surroundings of the deep acceptor due to the displacement of one of three C_s bonded with Al_{Si}-V_C. As a result, the differential equation describing the fluence dependence of the deep acceptor density, $N_{\mathrm{DA}}(\Phi)$, can be expressed as

$$\frac{\mathrm{d}N_{\mathrm{DA}}(\Phi)}{\mathrm{d}\Phi} = -\frac{\mathrm{d}N_{\mathrm{Al}}(\Phi)}{\mathrm{d}\Phi} - \kappa_{\mathrm{DA200}} N_{\mathrm{DA}}(\Phi) \tag{13}$$

where κ_{DA200} is the removal coefficient (or removal cross-section) of the deep acceptors for 200 keV electron irradiation. Figure 5 depicts the experimental $N_{\mathrm{DA}}(\Phi)$ and the simulated $N_{\mathrm{DA}}(\Phi)$ with κ_{DA200} of 1.0×10^{-17} cm^2 using Eq. (13), denoted by solid squares and the solid line, respectively. The simulation results in Fig. 5 show qualitative agreement with the experimental data.

Although N_{comp} was increased slightly with increasing Φ, it was less than 10^{15} cm^{-3}. This might be because V_C is increased by C_s displacement, that is, the displacement of one of four C_s bonded with one Si_s. However, the increment of V_C was too small to decrease the $p(T)$ by the irradiation. Consequently, the reduction in $p(T)$ by the 200 keV electron irradiation is mainly due to the decrease in N_{Al}, not to the increase in the density of V_C.

The following findings have been obtained from the study of 200 keV electron irradiation in Al-doped p-type 4H-SiC: (1) The reduction in $p(T)$ is greater than expected from the increase in V_C, (2) the reduction in $p(T)$ is mainly due to the decrease in N_{Al}, and (3) Al acceptors can be transformed into the deep acceptors with E_V +0.38 eV. These results suggest that the displacement of a C atom bonded with one Al atom and three Si atoms occurs much more easily than that of a C atom bonded with four Si atoms.

3.1.1.2 Hole Mobility

Figure 6 shows the $\mu_{\mathrm{h}}(T)$ for 200 keV electron irradiation with Φ of 0, 1×10^{16}, 3×10^{16}, and 7×10^{16} cm^{-2}. The $\mu_{\mathrm{h}}(T)$ decreased with increasing Φ between 0 and 3×10^{16} cm^{-2}, and then it was not changed. Compared with the decrement of $p(T)$ by 200 keV electron irradiation, the decrement of $\mu_{\mathrm{h}}(T)$ was a little.

In order to investigate which scattering mechanisms were affected by 200 keV electron irradiation, we simulated five kinds of temperature dependent mobility due to (1) acoustic phonon scattering, (2) nonpolar optical

Copyright 2017 KEI Journals. All Rights Reserved

phonon scattering, (3) polar optical phonon scattering, (4) ionized impurity scattering, and (5) neutral impurity scattering.[29,47]

The relaxation time for the acoustic phonon scattering, $\tau_{\mathrm{ac}}(E_{\mathrm{K}},T)$, is given by[29,48]

$$\frac{1}{\tau_{\mathrm{ac}}(E_{\mathrm{K}},T)}=\frac{\sqrt{2}m_{\mathrm{h}}^{*3/2}k_{\mathrm{B}}TD_{\mathrm{ac}}E_{\mathrm{K}}^{\ 1/2}}{\pi\hbar^{4}\rho v_{//}}, \quad (14)$$

where ρ is the mass density of atoms ($\rho = 3211\ \mathrm{kgm}^{-3}$ in SiC[49]), $v_{//}$ is the velocity of longitudinal acoustic phonons for the sound velocity along the hexagonal axis ($v_{//} = 13730$ m/s in SiC[50]), D_{ac} is the acoustic deformation potential, $\hbar$ is $h/2\pi$, and E_{K} is the kinetic energy.

The relaxation time for the nonpolar optical-phonon scattering valid for *p*-like wave functions, $\tau_{\mathrm{npo}}(E_{\mathrm{K}},T)$, is given by[29,51-53]

$$\frac{1}{\tau_{\mathrm{npo}}(E_{\mathrm{K}},T)}=\frac{D_{\mathrm{op}}^{\ 2}m_{dh}^{*\ 3/2}}{\sqrt{2}\pi\rho\hbar^{3}\omega_{\mathrm{nop}}}\times\{n(\omega_{\mathrm{nop}})(E_{K}+\hbar\omega_{\mathrm{nop}})^{1/2}+H(E_{K}-\hbar\omega_{\mathrm{nop}})[n(\omega_{\mathrm{nop}})+1]\times(E_{K}-\hbar\omega_{\mathrm{nop}})^{1/2}\}, \quad (15)$$

where $n(\omega_{\mathrm{nop}})$ is the phonon occupation factor of nonpolar optical phonons with an energy ($\hbar\omega_{\mathrm{nop}}$), given by the Bose distribution function

$$n(\omega_{\mathrm{nop}})=\frac{1}{\exp\left(\frac{\hbar\omega_{\mathrm{nop}}}{k_{\mathrm{B}}T}\right)-1}, \quad (16)$$

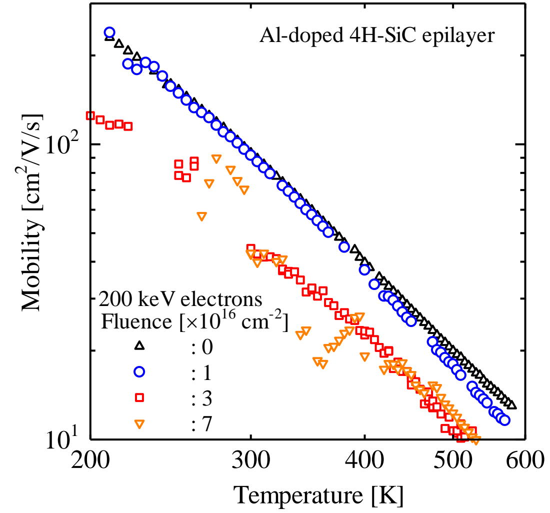

Figure 6. Temperature dependencies of hole mobilities for Al-doped 4H-SiC before and after irradiation with 200 keV electrons at three different fluences.

$H(E_{K}-\hbar\omega_{\mathrm{nop}})$ is the Heviside step function, D_{op} is the optical deformation potential. Here, $\hbar\omega_{\mathrm{nop}}$ is 0.10 eV,[29] which corresponds to an average energy of the optical-phonon modes at the Γ point of the Brillouin zone.[54]

The relaxation time for the polar optical phonon scattering, $\tau_{\mathrm{pop}}(E_{\mathrm{K}},T)$, derived by Callen,[55] is given by[29]

$$\frac{1}{\tau_{\mathrm{pop}}(E_{\mathrm{K}},T)}=\frac{1}{2}\cdot\frac{q^{2}\omega_{\mathrm{op}}}{4\pi\varepsilon_{\mathrm{p}}\hbar(2E_{\mathrm{K}}/m_{\mathrm{dh}}^{*})^{1/2}}\times\left\{n(\omega_{\mathrm{op}})\left(1+\frac{\hbar\omega_{\mathrm{op}}}{E_{\mathrm{K}}}\right)^{1/2}+H(E_{\mathrm{K}}-\hbar\omega_{\mathrm{op}})[n(\omega_{\mathrm{op}})+1]\left(1-\frac{\hbar\omega_{\mathrm{op}}}{E_{\mathrm{K}}}\right)^{1/2}\right.$$

Copyright 2017 KEI Journals. All Rights Reserved

$$+\frac{\hbar\omega_{\rm op}}{E_{\rm K}}\left[-n(\omega_{\rm op})\right]\sinh^{-1}\left[\left(\frac{E_{\rm K}}{\hbar\omega_{\rm op}}\right)^{1/2}\right]$$
$$+H\left(E_{\rm K}-\hbar\omega_{\rm op}\right)\frac{\hbar\omega_{\rm op}}{E_{\rm K}}\left[n\left(\omega_{\rm op}\right)+1\right]$$
$$\left.\times\sinh^{-1}\left[\left(\frac{E_{\rm K}}{\hbar\omega_{\rm op}}-1\right)^{1/2}\right]\right\} \qquad (17)$$

where $\hbar\omega_{\rm op}$ is the polar optical-phonon energy of 0.12 eV at small values of the phonon wave vector,[54] $\varepsilon_{\rm p}$ is determined by

$$\frac{1}{\varepsilon_{\rm p}}=\frac{1}{\varepsilon_{\infty}\varepsilon_0}-\frac{1}{\varepsilon_{\rm s}\varepsilon_0}, \qquad (18)$$

ε_{∞} is the very high-frequency relative dielectric constant ($\varepsilon_{\infty}=6.58$),[29,56] $\varepsilon_{\rm s}$ is the static relative dielectric constant ($\varepsilon_{\rm s}=9.78$), and ε_0 is the dielectric constant in vacuum. $n\left(\omega_{\rm op}\right)$ is the Bose distribution function;

$$n\left(\omega_{\rm op}\right)=\frac{1}{\exp\left(\frac{\hbar\omega_{\rm op}}{k_{\rm B}T}\right)-1}. \qquad (19)$$

The factor of 1/2 in Eq. (17) results from the *p*-like symmetry of the wave vector.[57]

The relaxation time for the ionized impurity scattering, $\tau_{\rm ii}(E_{\rm K},T)$, derived by Brooks and Herring,[58] is given by[29]

$$\frac{1}{\tau_{\rm ii}(E_{\rm K},T)}=\frac{2}{3}\cdot\frac{q^4N_{\rm ii}(T)L\left(2k\lambda_{\rm D}\right)}{16\pi\left(2m_{\rm h}^*\right)^{1/2}{\varepsilon_{\rm s}}^2{\varepsilon_0}^2}\cdot E_{\rm K}^{-3/2} \qquad (20)$$

and

$$L\left(2k\lambda_{\rm D}\right)=\ln\left(1+4k^2{\lambda_{\rm D}}^2\right)-\frac{4k^2{\lambda_{\rm D}}^2}{4k^2{\lambda_{\rm D}}^2+1}, \qquad (21)$$

where k is the electron wave vector assuming spherical parabolic bands and given by

$$k=\sqrt{\frac{2m_{\rm h}^*E_{\rm K}}{h^2}}, \qquad (22)$$

$\lambda_{\rm D}$ is the Debye screening length, given by

$$\lambda_{\rm D}=\sqrt{\frac{\varepsilon_{\rm s}\varepsilon_0k_{\rm B}T}{q^2p_{\rm sc}(T)}}, \qquad (23)$$

$p_{\rm sc}(T)$ is the screening hole concentration surrounding the ionized impurity, given by

$$p_{\rm sc}(T)=p(T)+\frac{\left(N_{\rm A}-N_{\rm D}-p(T)\right)\left(N_{\rm D}+p(T)\right)}{N_{\rm A}} \qquad (24)$$

$N_{\rm D}$ is the donor density, which is assumed to be $N_{\rm comp}$, and $N_{\rm A}$ is the acceptor density that is assumed to be $N_{\rm Al}+N_{\rm DA}$ in Al-doped p-type 4H-SiC.

The relaxation time for the neutral impurity scattering, $\tau_{\rm ni}(E_{\rm K},T)$, derived by Erginsoy's equation,[51,59] is given by

$$\frac{1}{\tau_{\rm ni}(E_{\rm K},T)}=\frac{10\varepsilon_{\rm s}\varepsilon_0N_{\rm ni}(T)h^3}{\pi^2{m_{\rm h}^*}^2q^2}, \qquad (25)$$

where $N_{\rm ni}(T)$ is the concentration of neutral impurities, given by

$$N_{\rm ni}(T)=N_{\rm A}-N_{\rm D}-p(T). \qquad (26)$$

By Matthiessen's rule,[60] the average total relaxation time, $\left\langle\tau_{\rm total}(T)\right\rangle$, is approximately described as

Copyright 2017 KEI Journals. All Rights Reserved

$$\frac{1}{\langle\tau_{\rm total}(T)\rangle} \cong \frac{1}{\langle\tau_{\rm ii}(T)\rangle} + \frac{1}{\langle\tau_{\rm ni}(T)\rangle} + \frac{1}{\langle\tau_{\rm ac}(T)\rangle} + \frac{1}{\langle\tau_{\rm pop}(T)\rangle} + \frac{1}{\langle\tau_{\rm npo}(T)\rangle}, \tag{27}$$

where each average relaxation time is calculated by

$$\langle\tau(T)\rangle = \frac{\int_0^\infty E_{\rm K}^{\;3/2}\tau(E_{\rm K},T)\exp\left(-\frac{E_{\rm K}}{kT}\right){\rm d}E_{\rm K}}{\int_0^\infty E_{\rm K}^{\;3/2}\exp\left(-\frac{E_{\rm K}}{kT}\right){\rm d}E_{\rm K}} \tag{28}$$

Finally, the drift mobility for holes perpendicular to the *c* axis is obtained by

$$\mu_{\rm total}(T) = \frac{q\langle\tau_{\rm total}(T)\rangle}{m_{h\perp}^*}, \tag{29}$$

where $m_{h\perp}^*$ is the hole effective mass in the basal plane, and $m_{h\perp}^* = 0.66m_0$.[61]

Figures 7-9 show the experimental and simulated temperature-dependent hole mobility for 200 keV electron irradiation with three fluences of 0, 1×10^{16}, and 3×10^{16} cm^{-2}, respectively. In the figures, solid, broken, doted, long-broken, dashed-dotted, dashed double-dotted lines represent the total mobility, and the mobilities for the acoustic phonon, nonpolar optical-phonon, polar optical-phonon, ionized impurity, and neutral impurity scattering, respectively. The total mobility is in good agreement with the experimental mobility.

According to Eq. (17), the mobility due to the polar optical phonon scattering

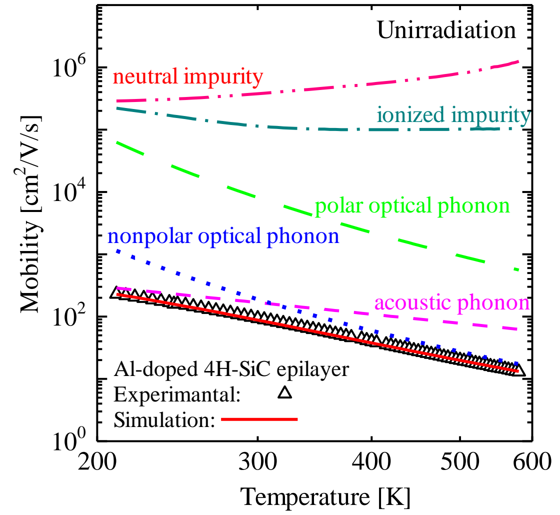

Figure 7. Experimental and simulated temperature-dependent hole mobilities for Al-doped 4H-SiC before irradiation.

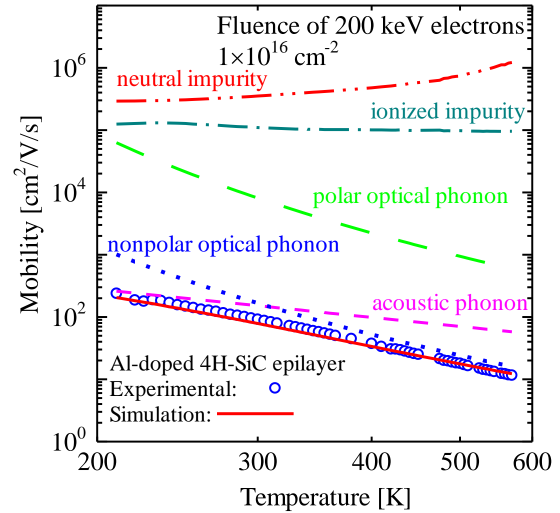

Figure 8. Experimental and simulated temperature-dependent hole mobilities for Al-doped 4H-SiC after 200 keV electron irradiation with fluence of 1×10^{16} cm^{-2}.

is not changed by electron irradiation, and is much larger than the experimental $\mu_{\rm h}(T)$. Although $p(T)$, $p_{\rm sc}(T)$, $N_{\rm A}$,

Copyright 2017 KEI Journals. All Rights Reserved

and N_D were changed by electron irradiation, the mobilities calculated from the ionized and neutral impurity scattering are much larger than the experimental $\mu_h(T)$. Therefore, they do not affect the experimental $\mu_h(T)$ at all, according to Matthiessen's rule. As a result, the acoustic phonon scattering affected the mobility at low temperatures, while the nonpolar optical-phonon scattering influenced the mobility at high temperatures.

Figure 10 depicts the changes of the temperature-dependent mobilities for the acoustic phonon and nonpolar optical-phonon scattering for 200 keV electron irradiation with three fluences of 0, 1×10^{16}, and 3×10^{16} cm^{-2}. The both mobilities were decreased with Φ between 0 and 3×10^{16} cm^{-2}.

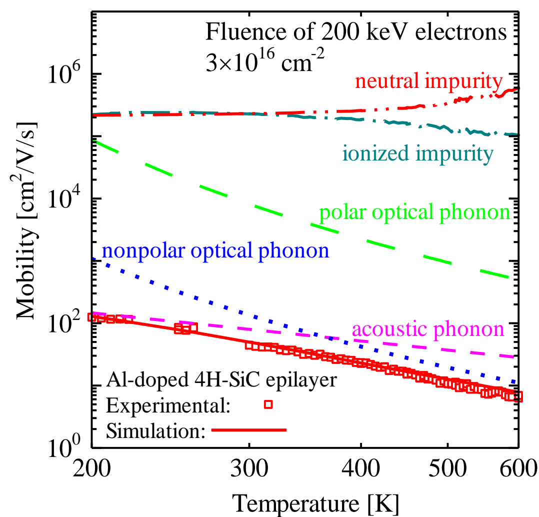

Figure 9. Experimental and simulated temperature-dependent hole mobilities for Al-doped 4H-SiC after 200 keV electron irradiation with fluence of 3×10^{16} cm^{-2}.

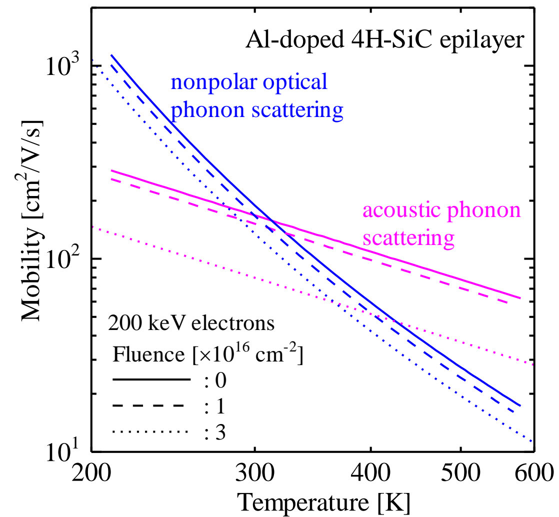

Figure 10. Changes of temperature-dependent hole mobilities for acoustic and nonpolar optical phonon scatterings for 200 keV electron irradiation with three fluences.

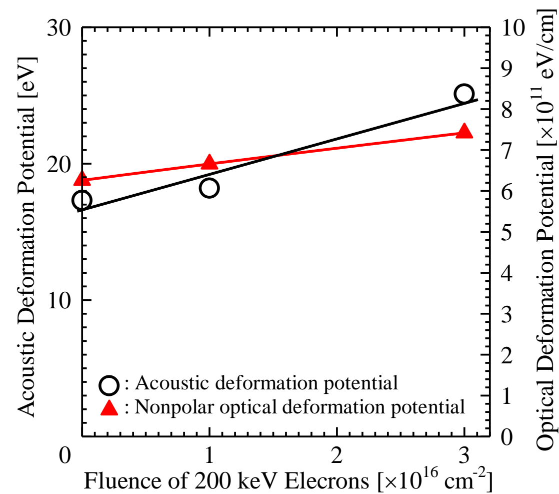

Figure 11. Fluence dependencies of D_{ac} or D_{op}.

Figure 11 shows the fluence dependencies of D_{ac} (circles) and D_{op} (triangles), indicating that D_{ac} and D_{op} are slightly increased with increasing Φ.

Copyright 2017 KEI Journals. All Rights Reserved

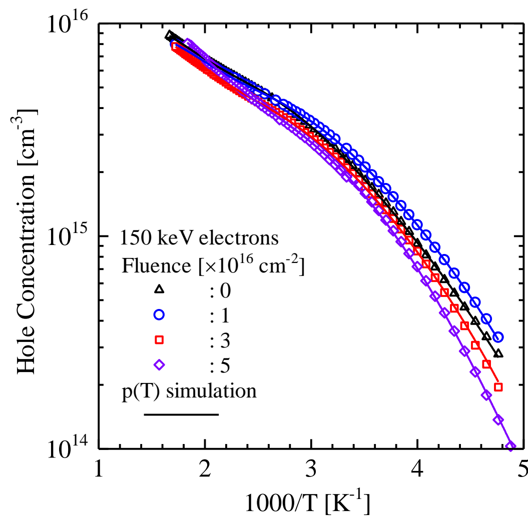

Figure 12. Temperature dependencies of hole concentrations for Al-doped 4H-SiC before and after irradiation with 150 keV electrons at three different fluences.

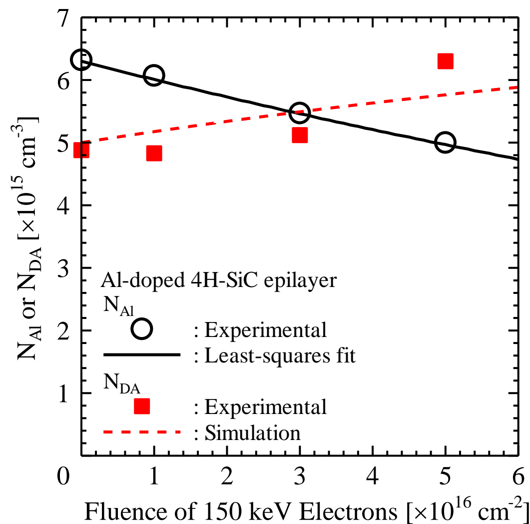

Figure 13. Fluence dependencies of shallow and deep acceptor densities.

These suggest that 200 keV electron irradiation influenced a lattice vibration.

3.1.2. 150 keV Electron Irradiation

Figure 12 shows the $p(T)$ before irradiation (circles) and after irradiation with 150 keV electrons at three fluences of 1×10^{16} (triangles), 3×10^{16} (squares), and 5×10^{16} cm^{-2} (diamonds). The $p(T)$ was slightly increased at low temperatures at the 1×10^{16} cm^{-2} fluence, and then is decreased with increasing Φ at $\geq 3\times10^{16}$ cm^{-2} fluences of 150 keV electron irradiation.

From each $p(T)$, two types of acceptor species were detected and evaluated using FCCS. The fluence dependencies of N_{Al} (circles) and N_{DA} (squares) are shown in Fig. 13. The N_{Al} decreased with increasing Φ, from which the removal cross section (κ_{Al150}) for 150 keV electron irradiation of the Al acceptor was determined to be 4.8×10^{-18} cm^2 by least-squares fitting. The solid curve in Fig. 13 represents the $N_{Al}(\Phi)$ calculated using Eq. (12), which is in good agreement with the experimental results shown by the circles.

The N_{DA}, on the other hand, increased experimentally with increasing Φ. The broken curve in Fig. 13 represents the $N_{DA}(\Phi)$ simulated with κ_{DA150} of 1.0×10^{-18} cm^2 using Eq. (13), which coincides qualitatively with the experimental fluence dependence of N_{DA} by 150 keV electron irradiation, denoted by squares.

3.2. N-doped 4H-SiC Epilayers

3.2.1. Lowly N-doped Samples

A 10-µm-thick N-doped n-type 4H-SiC epilayer on p$^+$-type 4H-SiC was

Copyright 2017 KEI Journals. All Rights Reserved

cut to a size of 3 mm × 3 mm. Four 100-nm-thick ohmic metal (Ni) dots were deposited by a vacuum vapor deposition method on the four corners of the surface of the sample, and the sample was then annealed at 1000 ºC in an Ar atmosphere. The $n(T)$ and $\mu_e(T)$ for samples irradiated with Φ of 0, 1×10^{16}, and 2×10^{16} cm^{-2} were obtained. The Hall-effect measurements were carried out twice at each fluence between 80 K and 300 K, and the $n(T)$ remained unchanged, indicating that any defects affecting $n(T)$ were not annealed at temperatures up to 300 K.

Figure 14 shows the experimental $n(T)$ before irradiation (triangles) and after irradiation by 200 keV electrons

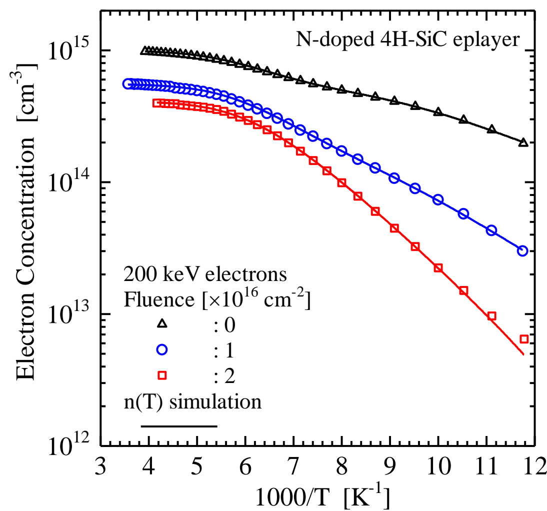

Figure 14. Temperature dependencies of electron concentrations for N-doped 4H-SiC before and after irradiation with 200 keV electrons at two different fluences.

with Φ of 1×10^{16} cm^{-2} (circles) and 2×10^{16} cm^{-2} (squares). From each experimental $n(T)$ shown in Fig. 14, two types of donor species were detected by FCCS, and the densities and energy levels of two donor species and N_{comp} were determined. In the light of the accuracy of Hall-effect measurements and FCCS analyses, the density values have two significant figures, and values larger than 10^{13} cm^{-3} are accurate. In the n-type case, N_{comp} is both N_{A} and the density of electron traps deeper than the energy levels of detected donors.

Two energy levels detected here correspond to the energy levels of the isolated, substitutional N donors at hexagonal and cubic C-sublattice sites.[25,35,62,63] The energy level of N donors at hexagonal C-sublattice sites (E_{NH}) was $E_{\mathrm{C}}-0.07$ eV, where E_{C} is the bottom of the conduction band. The energy level of N donors at cubic C-sublattice sites (E_{NK}) was $E_{\mathrm{C}}-0.12$ eV.

The corresponding densities were $N_{\mathrm{NH}}=5.1\times10^{14}$ and $N_{\mathrm{NK}}=4.7\times10^{14}$ cm^{-3}. As a result, $N_{\mathrm{NH}}\approx N_{\mathrm{NK}}$, which coincides with the expectation that N atoms equally occupy hexagonal and cubic C-sublattice sites because the number of hexagonal sites is equal to the number of cubic sites in 4H-SiC.

The electron concentration was simulated numerically by using the following equations:

Copyright 2017 KEI Journals. All Rights Reserved

$$n(T) + N_{\rm comp} = N_{\rm NH}\left[1 - f_{\rm FD,D}\left(E_{\rm NH}, T\right)\right] + N_{\rm NK}\left[1 - f_{\rm FD,D}\left(E_{\rm NK}, T\right)\right] \quad (30)$$

and

$$n(T) = N_{\rm C}(T)\exp\left[-\frac{E_{\rm C} - E_{\rm F}(T)}{k_{\rm B}T}\right], \quad (31)$$

where $f_{\rm FD,D}(E,T)$ is the Fermi-Dirac distribution function for donors, given by

$$f_{\rm FD,D}(E,T) = \frac{1}{1 + \frac{1}{g_{\rm D}}\exp\left[\frac{E - E_{\rm F}(T)}{k_{\rm B}T}\right]}, \quad (32)$$

$g_{\rm D} = 2$, and $N_{\rm C}(T)$ is the effective density of states in the conduction band, which is given by

$$N_{\rm C}(T) = 2\left(\frac{2\pi m_{\rm e}^{*} k_{\rm B}T}{h^2}\right)^{3/2} M_{\rm C}. \quad (33)$$

Further, $E_{\rm F}(T)$ is the Fermi level at T, $m_{\rm e}^{*}$ is the electron effective mass for the semiconductor, and $M_{\rm C}$ is the number of equivalent minima in the conduction band. Each solid curve in Fig. 14 is the result of an $n(T)$ simulation using the values of $N_{\rm NH}$, $E_{\rm NH}$, $N_{\rm NK}$, $E_{\rm NK}$, and $N_{\rm comp}$ for the corresponding Φ. The $n(T)$ simulations are in good agreement with the corresponding experimental results.

Figure 15 shows the fluence dependencies of $N_{\rm NH}$ (circles) and $N_{\rm NK}$ (squares), respectively. $N_{\rm NH}$ decreased substantially with increasing Φ, whereas $N_{\rm NK}$ decreased only slightly, indicating that N donors at hexagonal C-sublattice sites are less radiation-resistant than N donors at cubic C-sublattice sites. This finding suggests that 3C-SiC should be the most radiation-resistant and 6H-SiC should be the least radiation-resistant of N-doped 3C-SiC, 4H-SiC, and 6H-SiC.

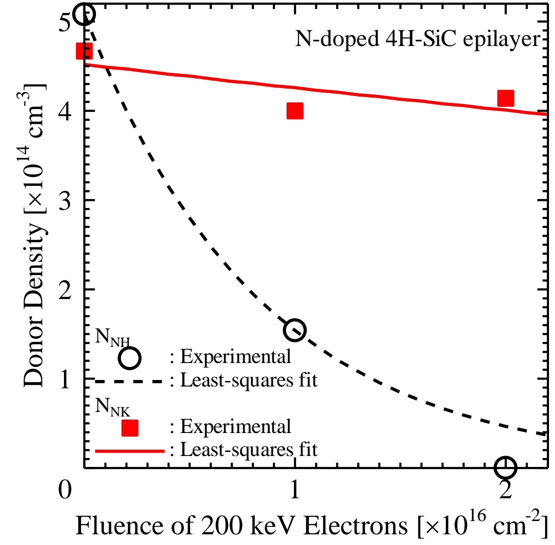

Figure 15. Fluence dependencies of shallow and deep donor densities.

Let us now consider other mechanism of the reduction in $n(T)$ by the 200 keV electron irradiation. The irradiation of 200 keV electrons can only displace C_s in SiC.[64-66] Therefore, V_C and an interstitial C (C_i) are created by the irradiation. With the rate of displacement of C_s by collision with 200 keV electrons, which is denoted by $\kappa_{\rm CD}$, the fluence dependence of the density of carbon-related defects (V_C or C_i), $N_{\rm CD}(\Phi)$, can be expressed as[11]

$$\frac{{\rm d}N_{\rm CD}(\Phi)}{{\rm d}\Phi} = \kappa_{\rm CD}. \quad (34)$$

Copyright 2017 KEI Journals. All Rights Reserved

Therefore,

$$N_{CD}(\Phi) = \kappa_{CD}\Phi + N_{CD}(0). \qquad (35)$$

In other words, κ_{CD} is the generation rate of carbon-related defects. The density of defects related to C_s displacement (i.e., $Z_{1/2}$ centers with $E_C - 0.65$ eV and $EH_{6/7}$ centers with $E_C - 1.55$ eV) has been reported to be nearly proportional to Φ,[67] as expected from Eq. (35). The HK4 center with $E_V + 1.44$ eV has been reported to be a complex including defects induced by C_s displacement.[64-66] According to studies of intrinsic defects in SiC,[68] the (0/+) level of V_C is at $E_V + 1.4$ eV and its (+/++) level is at $E_V + 1.68$ eV. Since the defects induced by C_s displacement are located around the middle of the band gap in SiC, they should act as electron traps in n-type SiC.

We now turn to the influence of $N_{CD}(\Phi)$ on $n(T)$. In order to simulate $n(T)$ for irradiated cases, the following assumptions are made: (1) the 200 keV electron irradiation does not change N_{NH}, E_{NH}, N_{NK}, and E_{NK} from their values at $\Phi = 0$ cm^{-2}, and (2) the irradiation only increases N_{comp} (that is, N_{comp} for an irradiated sample is the sum of N_{comp} for the non-irradiated case and the increase in $N_{CD}(\Phi)$ due to the irradiation).

Figure 16 shows the $n(T)$ simulations with N_{comp} of 0, 4.3×10^{14}, and 5.8×10^{14} cm^{-3}, which are used in order for the values of the $n(T)$ simulated at higher temperatures to be

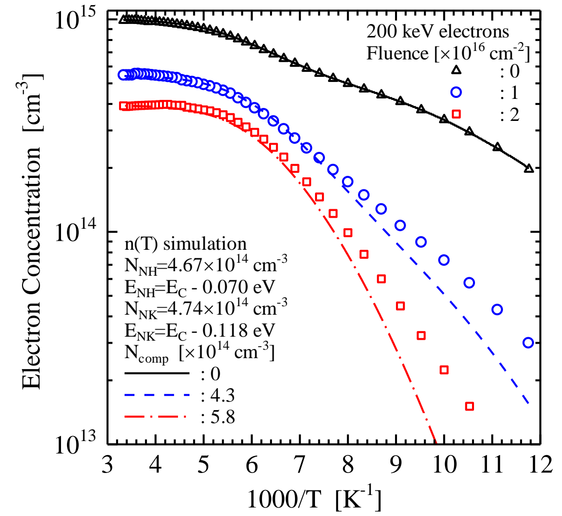

Figure 16. Simulations of temperature-dependent electron concentrations for three N_{comp}.

close to the experimental $n(T)$, denoted by solid, broken, and dashed-dotted curves, respectively. Also shown for comparison, the measurements of $n(T)$ for total fluences of 0, 1×10^{16} and 2×10^{16} cm^{-2}, denoted by triangles, circles, and squares, respectively, are shown. In the irradiated samples, at lower temperatures, the $n(T)$ simulation is much lower than the experimental $n(T)$.

In a comparison between Figs. 14 and 16, the deviation of the simulation curve from the experimental data is much larger in Fig. 16 than in Fig. 14. Therefore, it is clear that, although $n(T)$ does decrease with increasing N_{comp}, the reduction in $n(T)$ by electron irradiation cannot be explained by only an increase in the density of carbon-related defects.

Irradiation-induced defects in

Copyright 2017 KEI Journals. All Rights Reserved

N-doped n-type 4H-SiC have been intensively studied by DLTS.[65-67] By DLTS, deep-level defects with density much lower than the total density of N donors can be investigated.[11] On the other hand, changes in N-donor density due to irradiation can be investigated by FCCS. In this study, therefore, it is found that N donors are less radiation-resistant at hexagonal C-sublattice sites than at cubic C-sublattice sites.

By analogy with Eq. (11), the fluence dependencies of N_{NH} and N_{NK} are expected to be derived from the following differential equations:

$$\frac{\mathrm{d}N_{\mathrm{NH}}(\Phi)}{\mathrm{d}\Phi} = -\kappa_{\mathrm{NH200}} N_{\mathrm{NH}}(\Phi) \qquad (36)$$

and

$$\frac{\mathrm{d}N_{\mathrm{NK}}(\Phi)}{\mathrm{d}\Phi} = -\kappa_{\mathrm{NK200}} N_{\mathrm{NK}}(\Phi) \quad . \qquad (37)$$

Therefore,

$$N_{\mathrm{NH}}(\Phi) = N_{\mathrm{NH}}(0)\exp\left(-\kappa_{\mathrm{NH200}}\Phi\right) \quad (38)$$

and

$$N_{\mathrm{NK}}(\Phi) = N_{\mathrm{NK}}(0)\exp\left(-\kappa_{\mathrm{NK200}}\Phi\right), \quad (39)$$

where κ_{NH200} and κ_{NK200} are the removal cross-sections for 200 keV electron irradiation of the N donors at hexagonal and cubic C-sublattice sites, respectively. By fitting the curve to the experimental data, the values of κ_{NH200} and κ_{NK200} were determined to be 1.2×10^{-16} and 6.0×10^{-18} cm^2, respectively. The broken and solid curves in Fig. 15 represent the simulated $N_{\mathrm{NH}}(\Phi)$ and $N_{\mathrm{NK}}(\Phi)$, respectively.

This finding indicates that the density of N donors at hexagonal C-sublattice sites was reduced much more than the density of N donors at cubic C-sublattice sites. It is clear from Fig. 3 that C_s and a N atom (N_C) at a C-sublattice site can be displaced by 200 keV electron irradiation, suggesting that the threshold displacement energy of C_s or N_C at the hexagonal site is much lower than that at the cubic site.

In summary, the electron concentrations in lightly N-doped n-type 4H-SiC epilayers were decreased by 200 keV electron irradiation. The influence of the increase in the deep-level defect density as well as the decrease in donor density on the decrease in the electron concentration by irradiation was investigated using simulation results. Finally, this decrease in the electron concentration arose because the electron irradiation reduced the density of N donors. Moreover, the density of N donors at hexagonal C-sublattice sites was reduced much more than the density of N donors at cubic C-sublattice sites. This finding suggests that 3C-SiC should be the most radiation-resistant and 6H-SiC should be the least radiation-resistant of N-doped 3C-SiC, 4H-SiC, and 6H-SiC.

3.2.2. Highly N-doped Samples

A 10-μm-thick N-doped n-type 4H-SiC epilayer on p$^+$-type 4H-SiC was cut to a size of 3 mm × 3 mm. Four 100-nm-thick ohmic metal (Ni) dots were

Copyright 2017 KEI Journals. All Rights Reserved

deposited by a vacuum vapor deposition method on the four corners of the surface of the sample, and the sample was then annealed at 1000 ºC in an Ar atmosphere. The $n(T)$ and $\mu_e(T)$ for samples irradiated with Φ of 0, 1×10^{16}, and 3×10^{16} cm^{-2} were obtained. The Hall-effect measurements were carried out twice at each Φ between 85 K and 580 K, and the $n(T)$ remained unchanged, indicating that any defects affecting $n(T)$ were not annealed at temperatures up to 580 K.

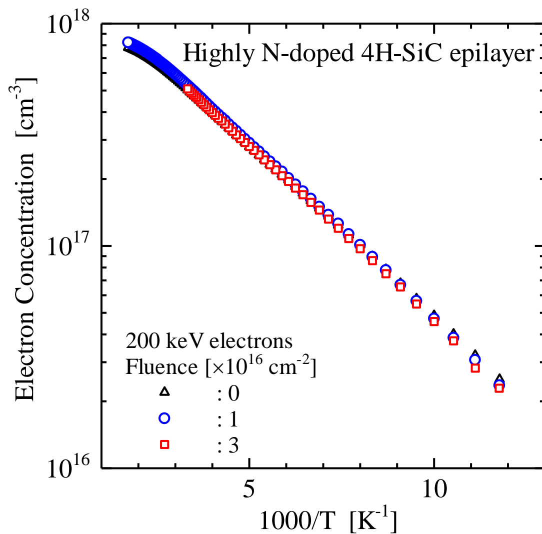

Figure 17. Temperature dependencies of electron concentrations for highly N-doped 4H-SiC before and after irradiation with 200 keV electrons at two different fluences.

Figure 17 shows the $n(T)$ in the highly N-doped 4H-SiC epilayer by 200 keV electrons with Φ of 0 (triangles), 1×10^{16} (circles), and 3×10^{16} cm^{-2} (squares). Although the $n(T)$ was a little decreased with increasing Φ, the ratio of decrement of $n(T)$ is much lower than that in lowly N-doped epilayers.

3.3. Al-doped 6H-SiC

3.3.1. Epilayers

A 4.9 μm-thick Al-doped p-type 4H-SiC epilayer on n$^+$-type 4H-SiC (resistivity: 0.027 Ω·cm) was cut to a size of 1×1 cm^2. Four ohmic metal (Ti/Al) dots were deposited by a sputtering method on the four corners of the surface of the sample, and then the sample was annealed at 900 ^{o}C for 1 min in an Ar atmosphere. The $p(T)$ and $\mu_h(T)$ were measured between 200 K and 600 K before irradiation, and then the sample was irradiated. After the Hall-effect measurement was carried out, the sample was again irradiated. The Hall-effect measurement and electron-irradiation were repeated. Although the Hall-effect measurements were carried out twice for each Φ, the $p(T)$ remained unchanged, indicating that any defects affecting $p(T)$ were not annealed at all for measurement temperature lower than 600 K.

Copyright 2017 KEI Journals. All Rights Reserved

A sample was irradiated by 200 keV electrons with Φ of 0, 1×10^{16}, 2×10^{16}, and 3×10^{16} cm^{-2}. However, the $p(T)$ at Φ of 3×10^{16} cm^{-2} could not be obtained. Another sample was irradiated with 100 keV electrons with Φ of 0, 1×10^{16}, 3×10^{16}, and 5×10^{16} cm^{-2}.

Figure 18 shows the $p(T)$ by 100 keV electron irradiation with Φ of 0, 1×10^{16}, 3×10^{16}, and 5×10^{16} cm^{-2}. By 100 keV electron irradiation, just like Al-doped 4H-SiC, the $p(T)$ was slightly increased, suggesting that the sample was considered to be annealed by heat due to electron irradiation.

Figure 19 shows the experimental $p(T)$ before irradiation (triangles) and after irradiation with 200 keV electrons at Φ of 1×10^{16} (circles) and 2×10^{16} cm^{-2} (squares). The $p(T)$ was significantly decreased by 200 keV electron irradiation. Because the $p(T)$ irradiated at Φ of 3×10^{16} cm^{-2} could not be measured, this sample was annealed at 500 °C (773 K) for 2 min in an Ar atmosphere, whose $p(T)$ was denoted by plus marks. By annealing, the $p(T)$ was significantly recovered.

As a result, 100 keV electrons could not displace any atoms at lattice sites in 6H-SiC, indicating that E_d in 6H-SiC should be larger than 20 eV.[45] As is clear from Fig. 3, 200 keV electrons can displace only C_s, neither Si_s nor Al_{Si}.

The values of N_{Al}, E_{Al}, N_{DA}, E_{DA}, and E_{comp} were determined by FCCS

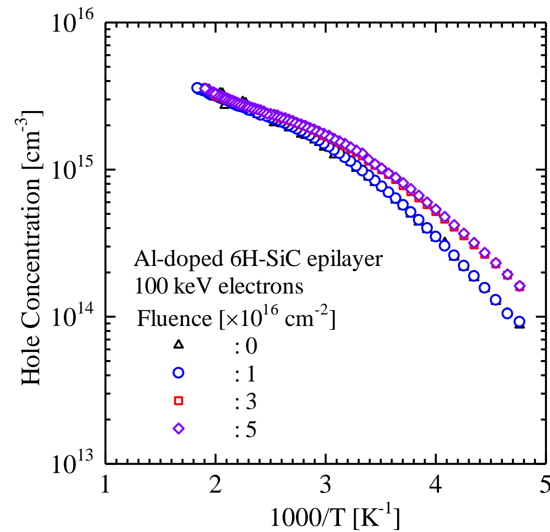

Figure 18. Temperature dependencies of hole concentrations for Al-doped 6H-SiC before and after irradiation with 100 keV electrons at three different fluences.

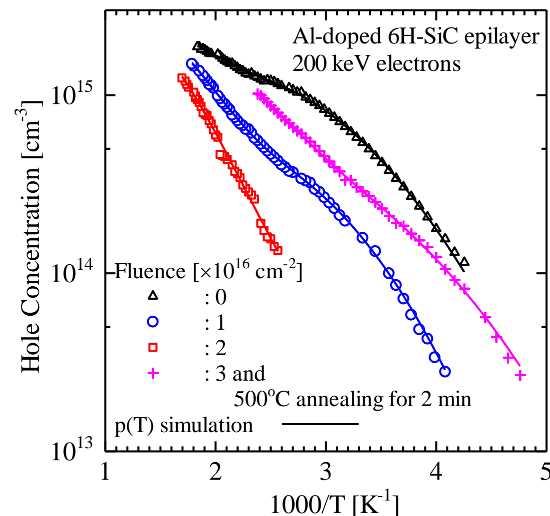

Figure 19. Temperature dependencies of hole concentrations for Al-doped 6H-SiC before and after irradiation with 200 keV electrons at two different fluences, and for 3×10^{16} cm^{-2} fluence irradiated sample annealed at 500 °C.

Copyright 2017 KEI Journals. All Rights Reserved

using the experimental $p(T)$. The $p(T)$ was numerically simulated by using Eqs. (6)-(10). Since the $p(T)$ simulations (solid curves) are in good agreement with the experimental $p(T)$ in Fig. 19, the values obtained by FCCS are reliable.

Figure 20 shows the fluence dependencies of N_{Al} and N_{DA}, denoted by circles and squares, respectively.

With irradiation by 200 keV electrons at Φ of 1×10^{16} cm^{-2}, the decrement of N_{Al} is nearly equal to the increment of N_{DA}, indicating that the irradiation transforms Al acceptors into the deep acceptors. The dependencies of N_{Al} and N_{DA} on Φ, simulated using Eqs. (11) and (13) with κ_{Al200} of 1.2×10^{-16} cm^2 and κ_{DA200} of 9.0×10^{-18} cm^2, are shown by the broken and solid curves, respectively. Compared with κ_{Al200} in 4H-SiC, κ_{Al200} in 6H-SiC is larger by 2.7, indicating that a $\mathrm{Al_{Si}}$-$\mathrm{C_s}$ bond in 6H-SiC is weaker than that in 4H-SiC. On the other hand, κ_{DA200} in 6H-SiC is nearly equal to κ_{DA200} in 4H-SiC.

After annealing the 3×10^{16} cm^{-2} fluence irradiated sample at 500 $^{\mathrm{o}}$C for 2 min, N_{Al} and N_{DA} could be determined. By annealing at 500 $^{\mathrm{o}}$C, N_{Al} was increased, and N_{DA} was decreased. From Fig. 20, furthermore, the increment of N_{Al} is nearly equal to the decrement of N_{DA}, suggesting that the 500 $^{\mathrm{o}}$C annealing transforms the deep acceptors into Al acceptors.

In the light of the results obtained by the irradiation and annealing, the deep acceptor is considered to be the $\mathrm{Al_{Si}}$-$\mathrm{V_C}$ complex. The 200 keV electron irradiation removes one of four $\mathrm{C_s}$ bonded with one $\mathrm{Al_{Si}}$ into an interstitial site, which creates the $\mathrm{Al_{Si}}$-$\mathrm{V_C}$ and an interstitial C ($\mathrm{C_i}$). Moreover, it removes one of three $\mathrm{C_s}$ bonded with $\mathrm{Al_{Si}}$-$\mathrm{V_C}$ into the interstitial site. As a result, the density of $\mathrm{Al_{Si}}$-$\mathrm{V_C}$ is decreased. This model leads to Eqs. (11) and (13)

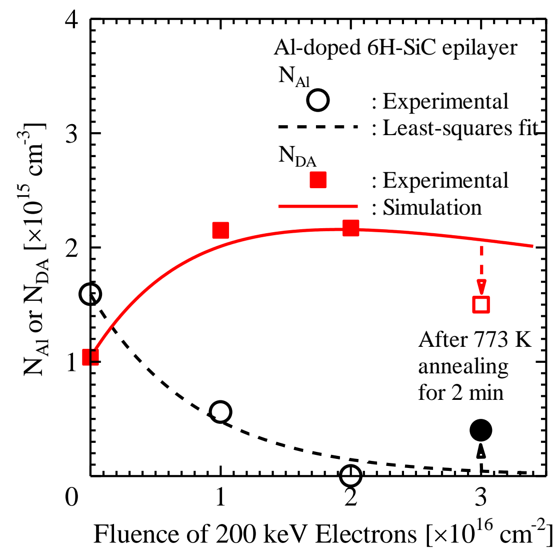

Figure 20. Fluence dependencies of shallow and deep acceptor densities.

Almost all defects were annealed out at higher than 750 $^{\mathrm{o}}$C.[46,67,69] Only a few defects were annealed out at 400 $^{\mathrm{o}}$C, and were reported to be related to $\mathrm{C_i}$.[46] Compared to $\mathrm{V_C}$, $\mathrm{C_i}$ is rather mobile but can migrate and react with other defects or impurities.[68] The 500 $^{\mathrm{o}}$C annealing, therefore, makes $\mathrm{C_i}$ migrate and react with $\mathrm{Al_{Si}}$-$\mathrm{V_C}$, which transforms $\mathrm{Al_{Si}}$-$\mathrm{V_C}$ to $\mathrm{Al_{Si}}$.

Copyright 2017 KEI Journals. All Rights Reserved

In summary, because the $p(T)$ was unchanged by irradiation with 100 keV electrons, 100 keV electrons could not displace any atoms at lattice sites in 6H-SiC. This indicated that E_d in SiC was higher than 20 eV, which meant that 200 keV electrons could not displace Al_{Si} and Si_s in Al-doped 6H-SiC. Therefore, 200 keV electrons could displace only C_s. By C_s displacement in Al-doped 6H-SiC, N_{Al} decreased monotonously with Φ, while N_{DA} initially increased and then decreased. By irradiation with 200 keV electrons with Φ of 1×10^{16} cm^{-2}, the decrement of N_{Al} was nearly equal to the increment of N_{DA}, while by 500 °C annealing the increment of N_{Al} was nearly equal to the decrement of N_{DA}.

3.3.2. Al-Implanted Layers

In order to form a p-type 6H-SiC layer, Al ions were implanted at 800 °C in a 4.9-µm-thick n-type 6H-SiC epilayer with a N-doping level of 6.7×10^{15} cm^{-3} on an n$^+$-type 6H-SiC substrate. To obtain a 0.5-µm-thick box profile of Al concentration, fivefold Al ion implantation was carried out using 20, 50, 110, 200, and 340 keV onto the n-type SiC epilayer surface. After the implantation, the sample of 5×5 cm^2 size was annealed at 1700 °C for 30 min in an Ar atmosphere. Four ohmic metal (Al/Ti) dots were deposited by a sputtering method on the four corners of the surface of the sample, and the sample was annealed at 900 °C for 1 min in an Ar atmosphere to form good ohmic contacts.

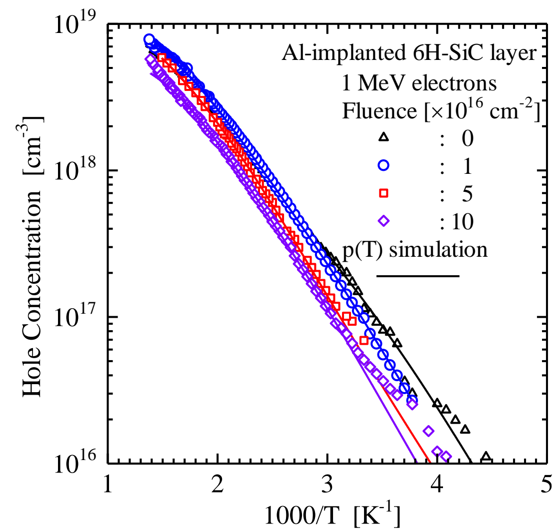

Figure 21. Temperature dependencies of hole concentrations for Al-implanted 6H-SiC before and after irradiation with 1 MeV electrons at three different fluences.

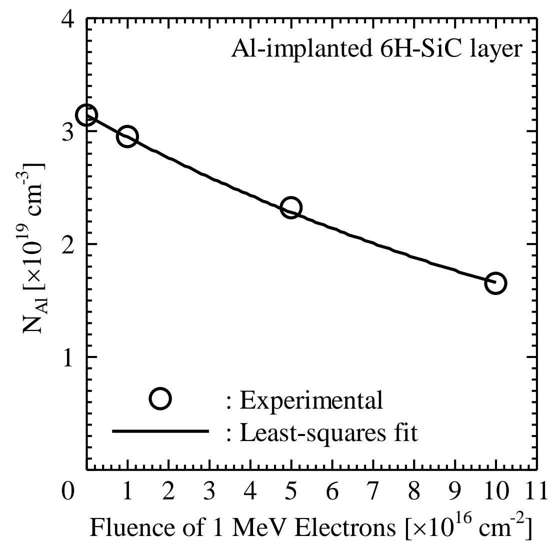

Figure 22. Fluence dependence of acceptor density.

The fluences of 1 MeV electrons were of 0, 1×10^{16}, 5×10^{16}, and 1×10^{17} cm^{-2}. The $p(T)$ was measured in the

Copyright 2017 KEI Journals. All Rights Reserved

temperature range from 210 to 720 K.

The hole concentration is expected to be reduced by the increase in the density of deep-level defects as well as the decrease in the density of Al acceptors. Therefore, we evaluated these densities in order to determine the main cause of the reduction in $p(T)$.

Figure 21 shows the $p(T)$ for the unirradiated and irradiated p-type 6H-SiC layers. Using each $p(T)$ in Fig. 21, the values of acceptor densities and levels, and E_{comp} were determined by FCCS. In the analysis of $p(T)$, the excited states of Al acceptors should be considered, because the Al concentration (C_{Al}) measured by SIMS was higher than 1×10^{18} cm^{-3} in these implanted layers.[70-74] Moreover, there is one acceptor level (E_{Al}) in heavily Al-doped SiC (C_{Al} of $>1\times10^{18}$ cm^{-3}), while there are two acceptor levels (E_{Al} and E_{DA}) in the case of $C_{\mathrm{Al}}<1\times10^{18}$ cm^{-3}.[24]

In the case of heavily-doped p-type wide bandgap semiconductors, instead of $f_{\mathrm{FD,A}}(E_{\mathrm{A}})$ in Eq. (8), the distribution function ($f_{\mathrm{ex}}(E_{\mathrm{A}},T)$) including the first-to-($n-1$)th excited states of the acceptor is used, and described as[70-81]

$$f_{\mathrm{ex}}(E_{\mathrm{A}},T)=\frac{1}{1+g_{\mathrm{ex}}(T)\exp\left[\dfrac{E_{\mathrm{A}}-E_{\mathrm{F}}(T)}{k_{\mathrm{B}}T}\right]} \quad (40)$$

where $g_{\mathrm{ex}}(T)$ is the degeneracy factor for acceptors, given by

$$g_{\mathrm{ex}}(T)=g_{\mathrm{A}}\exp\left(-\frac{\overline{E_{\mathrm{ex}}(T)}}{k_{\mathrm{B}}T}\right)\times\left[1+\sum_{r=2}^{n}g_r\exp\left(\frac{E_r-E_{\mathrm{A}}}{k_{\mathrm{B}}T}\right)\right], \quad (41)$$

$\overline{E_{\mathrm{ex}}(T)}$ is the ensemble average of its ground and excited state levels, given by

$$\overline{E_{\mathrm{ex}}(T)}=\frac{\sum_{r=2}^{n}(E_{\mathrm{A}}-E_r)g_r\exp\left(-\dfrac{E_{\mathrm{A}}-E_r}{k_{\mathrm{B}}T}\right)}{1+\sum_{r=2}^{n}g_r\exp\left(-\dfrac{E_{\mathrm{A}}-E_r}{k_{\mathrm{B}}T}\right)} \quad (42)$$

g_r is the ($r-1$)th excited state degeneracy factor, given by

$$g_r=r^2, \quad (43)$$

and E_r is the ($r-1$)th excited state level, which is given by

$$\begin{aligned}E_r&=\frac{q^4m_{\mathrm{h}}^*}{8h^2\varepsilon_{\mathrm{s}}^2\varepsilon_0^2r^2}+E_{\mathrm{V}}\\&=13.6\frac{m_{\mathrm{h}}^*}{m_0\varepsilon_{\mathrm{s}}^2r^2}+E_{\mathrm{V}}\quad[\mathrm{eV}]\end{aligned}. \quad (44)$$

The $p(T)$ was numerically simulated by using

$$p(T)+N_{\mathrm{comp}}=N_{\mathrm{Al}}f_{\mathrm{ex}}(E_{\mathrm{Al}},T). \quad (45)$$

In Fig. 21, the $p(T)$ simulations are described by solid curves, which is in good agreement with the experimental $p(T)$.

The values of the acceptor level obtained by FCCS using $f_{\mathrm{ex}}(E_{\mathrm{A}},T)$ were independent of Φ, and were approximately $E_{\mathrm{V}}+0.22$ eV, indicating that this acceptor species is an Al

Copyright 2017 KEI Journals. All Rights Reserved

acceptor (Al_{Si}).

Figure 22 depicts the dependence of N_{Al} on Φ. The density of Al acceptors is decreased by the displacement of Al atoms or their nearest neighbor C atoms because only the Al atom bonding to four C atoms works as an Al acceptor. Since the number of collisions between incident electrons and those atoms in unit volume is proportional to N_{Al}, the following differential equation describing the fluence dependence of the Al acceptor density, $N_{\mathrm{Al}}(\Phi)$, is obtained:

$$\frac{\mathrm{d}N_{\mathrm{Al}}(\Phi)}{\mathrm{d}\Phi} = -\kappa_{\mathrm{Al1000}} N_{\mathrm{Al}}(\Phi), \qquad (46)$$

where κ_{Al1000} is the removal cross-section of Al acceptors for 1 MeV electron irradiation and Φ is the fluence of 1 MeV electrons. Therefore,

$$N_{\mathrm{Al}}(\Phi) = N_{\mathrm{Al}}(0)\exp(-\kappa_{\mathrm{Al1000}}\Phi). \qquad (47)$$

In Fig. 22, the solid curve is the fit obtained by the least-square method. Because the experimental data agree quite well with the theoretical model, $\kappa_{\mathrm{Al1000}}$is determined as 6.4×10^{-18} cm^2.

The values of N_{comp} are of the order of 10^{17} cm^{-3}, which are much lower than N_{Al}. This indicates that the reduction in $p(T)$ by the irradiation is mainly due to the decrease in N_{Al}, not to the increase in the density of deep-level defects. Furthermore, the surroundings of Al acceptors are considered to be more easily changed by irradiation than the surroundings of the SiC matrix.

In summary, we investigated the $p(T)$ in Al-implanted p-type 6H-SiC before and after 1 MeV electron irradiation as a function of Φ. Using $p(T)$, the acceptor density and level in the bandgap were determined by FCCS in consideration of the excited states of Al acceptors. As determined from the acceptor level, this acceptor species was assigned to Al. The reduction in $p(T)$ by electron irradiation was mainly due to the decrease in the density of Al acceptors, not to the increase in the density of deep-level defects. Therefore, the surroundings of Al acceptors were changed by electron irradiation more easily than the surroundings of the SiC matrix.

Conclusions

Electron-irradiation damage in Al-doped 4H-SiC epilayers, N-doped 4H-SiC epilayers, Al-doped 6H-SiC epilayers, and Al-implanted 6H-SiC layers was investigated using Hall-effect measurements. The Hall-effect measurements tell us the changes of the majority-carrier concentration and mobility, while DLTS gives the changes of deep-level densities much less than the majority-carrier concentration. From the temperature dependence of the majority-carrier concentration, FCCS can determine the densities and energy levels of dopants and defects.

Irradiation of electrons with ≥ 150 keV decreased the majority-carrier concentration, while 100 keV electron

Copyright 2017 KEI Journals. All Rights Reserved

irradiation could not change it. The decrease in the hole concentration in Al-doped SiC by 200 keV electron irradiation resulted from the decrease in the density of Al acceptors with $E_V + 0.22$ eV. Since 200 keV electron irradiation could displace C_s, neither Si_s nor Al_{Si} in Al-doped SiC, the decrement of the Al acceptor density came from the displacement of one of four C_s bonded with Al_{Si}. The displacement of C_s made another deep acceptor with $E_V + 0.38$ eV.

The decrease in the electron concentration in N-doped SiC by 200 keV electron irradiation resulted mainly from the decrease in the density of N donors at hexagonal C-sublattice sites with $E_C - 0.07$ eV, not the density of N donors at cubic C-sublattice sites with $E_C - 0.12$ eV. Since 200 keV electron irradiation could displace C_s and N_C, not Si_s in N-doped SiC, the displacement of N_C resulted in the decrement of donor densities, and the N donors at cubic C-sublattice sites have radiation resistance more than the N donors at hexagonal C-sublattice sites.

Acknowledgments

The author would like to thank Dr. S. Onoda, Dr. T. Ohshima, and Dr. H. Itoh of Japan Atomic Energy Agency for the electron irradiation, and the graduate and undergraduate students in Matsuura laboratory of Osaka Electro-Communication University, especially Mr. K. Nishikawa, Mr. S. Kagamihara, Mr. N. Minohara, Mr. K. Izawa, Mr. H. Yanagisawa, Mr. K. Nishino, Mr. T. Nojiri, and Mr. K. Murata for the Hall-effect measurements of the electron-irradiated samples, and Mr. K. Murata for the simulation of mobility.

This work was partially supported by the Academic Frontier Promotion Projects of the Ministry of Education, Culture, Sports, Science and Technology in 1998-2002 and 2003-2007, and partially supported by a Grant-in-Aid for Scientific Research (C) of the Japan Society for the Promotion of Science in 2006 and 2007 (18560356).

References

1. A. L. Barry, B. Lehman, D. Fritsch, and D. Bräuning, IEEE Trans. Nucl. Sci. **38**, 1111 (1991).
2. S. M. Sze, “Physics of Semiconductor Devices” (Wiley, New York, 1981) 2nd ed., p.38 and p.214.
3. T. Hisamatsu, O. Kawasaki, S. Matsuda, T. Nakao, and Y. Wakow, Solar Energy Mater. Solar Cells **50**, 331 (1998).
4. H. Matsuura, Y. Uchida, T. Hisamatsu, and S. Matsuda, Jpn. J. Appl. Phys., Part 1 **37**, 6034 (1998).
5. H. Matsuura, Y. Uchida, N. Nagai, T. Hisamatsu, T. Aburaya, and S. Matsuda, Appl. Phys. Lett. **76**, 2092 (2000).

Copyright 2017 KEI Journals. All Rights Reserved

6. H. Matsuura, H. Iwata, S. Kagamihara, R. Ishihara, M. Komeda, H. Imai, M. Kikuta, Y. Inoue, T. Hisamatsu, S. Kawakita, T. Ohshima, and H. Itoh, Jpn. J. Appl. Phys., Part 1 **45**, 2648 (2006).
7. A. Hallén, A. Henry, P. Pellegrino, B. G. Svensson, and D. Åberg, Mater. Sci. Eng. B **61-6**2, 378 (1999).
8. D. Åberg, A. Hallén, P. Pellegrino, and B. G. Svensson, Appl. Phys. Lett. **78**, 2908 (2001).
9. H. Matsuura, K. Aso, S. Kagamihara, H. Iwata, T. Ishida, and K. Nishikawa, Appl. Phys. Lett. **83**, 4981 (2003).
10. H. Matsuura, S. Kagamihara, Y. Itoh, T. Ohshima, and H. Itoh, Physica B **376-377**, 342 (2006).
11. H. Matsuura, N. Minohara, and T. Ohshima, J. Appl. Phys. **104**, 043702 (2008).
12. H. Matsuura, N. Minohara, Y. Inagawa, M. Takahashi, T. Ohshima, and H. Itoh, Mater. Sci. Forum **556-557**, 379 (2007).
13. D. V. Lang, J. Appl. Phys. **45**, 3023 (1974).
14. D. K. Schroder, "Semiconductor Materials and Device Characterization" (Wiley, New York, 1998) 2nd ed., pp. 276 and 290.
15. H. Matsuura, "Determination Methods of Densities and Energy Levels of Impurities and Defects Affecting Majority-Carrier Concentration in Next-Generation Semiconductors" in "Advances in Condensed Matter and Materials Research, Vol. 10", edited by H. Geelvinck and S. Reynst (Nova Science Publishers, New York, 2011), Chaptor 7.
16. H. Matsuura, T. Okuno, H. Okushi, and K. Tanaka, J. Appl. Phys. **55**, 1012 (1984).
17. H. Matsuura, J. Appl. Phys. **64**, 1964 (1988).
18. H. Matsuura, IEEE Trans Electron Devices **36**, 2908 (1989).
19. H. Matsuura, "Junction properties of amorphous semiconductors" in "Glow-Discharge Hydrogenated Amorphous Silicon", edited by K. Tanaka (KTK Sci. Pub., Tokyo, 1989), Chapter 10.
20. H. Matsuura, J. Appl. Phys. **68**, 1138 (1990).
21. H. Matsuura and H. Okushi, "Electrical properties of amorphous/crystalline-semiconductor heterojunctions" in Amorphous and Micro-Crystalline Semiconductor Devices Vol. II: Materials and Device Physics, edited by J. Kanicki (Artech House, Boston, 1992), Chapter 11.
22. H. Matsuura, Y. Masuda, Y. Chen, and S. Nishino, Jpn. J. Appl. Phys. Part 1 **39**, 5069 (2000).
23. H. Matsuura, K. Morita, K. Nishikawa, T. Mizukoshi, M. Segawa,

Copyright 2017 KEI Journals. All Rights Reserved

and W. Susaki, Jpn. J. Appl. Phys., Part 1 **41**, 496 (2002).

24. H. Matsuura, M. Komeda, S. Kagamihara, H. Iwata, R. Ishihara, T. Hatakeyama, T. Watanabe, K. Kojima, T. Shinohe, and K. Arai, J. Appl. Phys. **96**, 2708 (2004).
25. S. Kagamihara, H. Matsuura, T. Hatakeyama, T. Watanabe, M. Kushibe, T. Shinohe, and K. Arai, J. Appl. Phys. **96**, 5601 (2004).
26. H. Matsuura, H. Nagasawa, K. Yagi, and T. Kawahara, J. Appl. Phys. **96**, 7346 (2004).
27. H. Matsuura and K. Nishikawa, J. Appl. Phys. **97**, 093711 (2005).
28. H. Matsuura, J. Mater. Sci.: Mater. Electron. **19**, 810 (2008).
29. A. Koizumi, J. Suda, and T. Kimoto, J. Appl. Phys. **106**, 013716 (2009).
30. H. Matsuura, K. Aso, S. Kagamihara, H. Iwata, T. Ishida, and K. Nishikawa, Mater. Sci. Forum **457-460**, 751 (2004).
31. H. Matsuura, S. Kagamihara, Y. Itoh, T. Ohshima, and H. Itoh, Microelectronic Eng. **83**, 17 (2006).
32. H. Matsuura, K. Izawa, N. Minohara, T. Ohshima, Jpn. J. Appl. Phys. **47**, 5355 (2008).
33. H. Matsuura, H. Yanagisawa, K. Nishino, Y. Myojin, T. Nojiri, Y. Matsuyama, and T. Ohshima, Physica B **404**, 4755 (2009).
34. H. Matsuura, H. Yanagisawa, K. Nishino, T. Nojiri, Y. Myojin, Y. Matsuyama, S. Onoda, and T. Ohshima, Open Appl. Phys. J. **4**, 37 (2011).
35. M. Ikeda, H. Matsunami, and T. Tanaka, Phys. Rev. B 22, 2842 (1980).
36. T. Troffer, M. Schadt, T. Frank, H. Itoh, G. Pensl, J. Heindl, H. P. Strunk, and N. Maier, Phys. Status Solidi A **162**, 277 (1997).
37. C. M. Zetterling, “Process Technology for Silicon Carbide Devices”, (INSPEC, London, 2002), p. 54.
38. A. Schöner, K. Rottner, N. Nordell, Mater. Res. Symp. Proc. **423**, 661 (1996).
39. A. Gali, P. Deák, R. P. Devaty, W. J. Choyke, Phys. Rev. B **60**, 10620 (1999).
40. I. V. Ilyin, E. N. Mokhov, P. G. Baranov, Mater. Sci. Forum **353–356**, 521 (2001).
41. T. Egilsson, J. P. Bergman, I. G. Ivanov, A. Henry, and E. Janzén, Phys. Rev. B **59**, 1956 (1999).
42. J. W. Cobett, “Electron Radiation Damage in Semiconductors and Metals”, edited by F. Seitz and D. Turnbull (Academic Press, New York, 1966), p. 6.
43. H. Inui, H. Mori, and H. Fujita, Mag. B **61**, 107 (1990).

Copyright 2017 KEI Journals. All Rights Reserved

44. A. A. Rempel, W. Sprengel, K. Blaurock, K. J. Reichle, J. Major, and H.-E. Schaefer, J. Appl. Phys. **89**, 185501 (2002).
45. H. J. von Bardeleben, J. L. Cantin, L. Henry, and M. F. Barthe, Phys. Rev. B **62**, 10841 (2000).
46. L. Storasta, J. P. Bergman, E. Janzén, A. Henry, and J. Lu, J. Appl. Phys. **96**, 4909 (2004).
47. S. Contreras, L. Konczewicz, R. Arvinte, H. Peyre, T. Chassagne, M. Zielinski, and S. Juillaguet, Phys. Status Solidi A **214**, 1600679 (2017).
48. M. Costato, G. Gagliani, C. Jacoboni, and L. Reggiani, J. Phys. Chem. Solids **35**, 1605 (1974).
49. A. H. G. de Mesquita, Acta Crystallogr. **23**, 610 (1967).
50. S. Karmann, R. Helbig, and R. A. Stein, J. Appl. Phys. **66**, 3922 (1989).
51. B. K. Ridley, "Quantum Processes ion Semiconductors", 4th ed. (Clarendon, Oxford, 1999).
52. D. C. Look, "Electrical Characterization of GaAs Materials and Devices", (Wiley, New York, 1989).
53. E. M. Conwell and M. O. Vassell, Phys. Rev. **166**, 797 (1968).
54. D. W. Feldman, J. J. H. Parker, W. J. Choyke, and L. Partrick, Phys. Rev. **173**, 787 (1968).
55. H. B. Callen, Phys. Rev. **76**, 1394 (1946).
56. L. Partrick and W. J. Choyke, Phys. Rev. B **2**, 2255 (1970).
57. J. D. Wiley, Phys. Rev. B **4**, 2485 (1971).
58. H. Brooks, "Advances in Electronic and Electron Physics" (Academic, New York, 1955), Vol. **7**, pp. 85-182.
59. C. Erginsoy, Phys. Rev. **79**, 1013 (1950).
60. B. L. Anderson and R. L. Anderson, "Fundamentals of Semiconductor Devices", (McGraw Hill, New York, 2005), p. 122.
61. N. T. Son, P. N. Hai, W. M. Chen, C. Hallin, B. Monermar, and E. Janzén, Phys. Rev. B **61**, R10544 (2000).
62. W. Götz, A. Schöner, G. Pensl, W. Suttrop, W. J. Choyke, R. Stein, and S. Leibenznder, J. Appl. Phys. **73**, 3332 (1993).
63. G. L. Harris, "Properties of Silicon Carbide", (INSPEC, London, 1995).
64. J. W. Steeds, F. Carosella, G. A. Evans, M. M. Ismail, L. R. Danks, W. Voegeli, Mater. Sci. Forum **353-356**, 381-4 (2001).
65. L. Storasta, J. P. Bergman, E. Janzén, A. Henry, J. Lu, J. Appl. Phys. **96**, 4909 (2004).
66. K. Danno and T. Kimoto, J. Appl. Phys. **100**, 113728 (2006).
67. K. Danno and T. Kimoto, Mater. Sci. Forum **556-557**, 331 (2007).

Copyright 2017 KEI Journals. All Rights Reserved

68. W. J. Choyke, H. Matsunami, and G. Pensl, “Silicon Carbide”, (Springer, Berlin, 2004).
69. M. Gong, S. Fung, C.D. Beling, Z. You, J. Appl. Phys. **85**, 7604 (1999).
70. H. Matsuura, New J. Phys. **4**, 12 (2002).
71. H. Matsuura, J. Appl. Phys. **95**, 4213 (2004).
72. H. Matsuura and K. Nishikawa, J. Appl. Phys. **97**, 093711 (2005).
73. H. Matsuura, Phys. Rev. B **74**, 245216 (2006).
74. H. Matsuura, K. Sugiyama, K. Nishikawa, T. Nagata, and N. Fukunaga, J. Appl. Phys. **94**, 2234 (2003).
75. H. Matsuura, D. Katsuya, T. Ishida, S. Kagamihara, K. Aso, H. Iwata, T. Aki, S.-W. Kim, T. Shibata, and T. Suzuki, phys. stat. sol. C **0**, 2214 (2003).
76. H. Matsuura, Inst. Phys. Conf. Ser. No. 184, 329 (2004).
77. H. Matsuura, Electrochemical Soc. Proc. **2004-06**, 570 (2004).
78. H. Matsuura, T. Morizono, Y. Inoue, S. Kagamihara, A. Namba, T. Imai, and T. Takabe, Jpn. J. Appl. Phys. **45**, 6376 (2006).
79. H. Matsuura, J. Mater. Sci.: Mater. Electron. **19**, 720 (2008).
80. H. Matsuura, T. Morine, and S. Nagamachi, Mater. Sci. Forum **778-780**, 685 (2014).
81. H. Matsuura, T. Morine, and S. Nagamachi, Acta Physica, Polonica A **125**, 1017 (2014).

Copyright 2017 KEI Journals. All Rights Reserved